INORGANIC CHEMISTRY FRONTIERS

RESEARCH ARTICLE

View Article Online
View Journal | View Issue

Cite this: *Inorg. Chem. Front.*, 2022, **9**, 3130

Bimetallic sulfide particles incorporated in Fe/Co-based metal–organic framework ultrathin nanosheets toward boosted electrocatalysis of the oxygen evolution reaction†

Rui Yu,[a] Cheng Wang,[a] Dongmei Liu,[a] Zhengying Wu, *[b] Jie Li[a] and Yukou Du *[a]

The development of inexpensive, high-performance, and long-lasting electrocatalysts toward the oxygen evolution reaction (OER) has been proved to be crucial to enhance the efficiency of water splitting to obtain clean and sustainable energy. Herein, Fe/Co-based metal–organic framework (MOF) ultrathin nanosheets doped with (Fe)-Co_3S_4 metal sulfide (MS) particles (CoFe-MS/MOF) are reported as superior electrocatalysts for the OER. CoFe-MS/MOFs exhibit an outstanding OER performance with a small overpotential of 261 mV and a low Tafel slope of 60.3 mV dec^{-1} at a current density of 10 mA cm^{-2} while showing high durability in an alkaline medium. The existence of metal sulfide particles plays a pivotal part in promoting the charge transfer capacity as well as the formation of ultrathin MOF nanosheets. More significantly, they can also modulate the adsorption energy of oxygenated intermediates, thereby significantly enhancing the inherent electrocatalytic activity. This work provides guidance for rationally designing and synthesizing inexpensive and highly active bimetallic sulfide doped MOF electrocatalysts in the electrochemical energy field.

Received 15th January 2022,
Accepted 29th April 2022

DOI: 10.1039/d2qi00125j

rsc.li/frontiers-inorganic

1. Introduction

Due to severe environmental pollution and energy depletion resulting from extensive consumption of fossil energy, numerous researches have been dedicated to developing sustainable and clean energy sources,[1–4] among which, water electrolysis for the production of hydrogen is an eco-friendly and economically viable strategy.[5–7] Nevertheless, the sluggish OER severely affects the efficiency of overall water splitting. Since OER is a thermodynamically unfavorable process involving the transfer of four proton-coupled electron, it is a bottleneck for water splitting.[8–10] Therefore, exploring efficient OER electrocatalysts is a key requirement for accelerating the reaction by reducing the activation energy, and thus achieving an improvement of energy conversion efficiency.[11] Although Ir/Ru-based precious metal materials remain the state-of-the-art electrocatalysts toward OER by far, the scarcity, inferior durability and high cost severely limit their large-scale industrial application.[12,13] As a consequence, development of efficient, cost-effective, and stable noble-metal-free electrocatalysts toward the OER is of considerable scientific and research significance.[14,15]

In recent years, a large amount of research has been dedicated to exploiting highly efficient and cost-effective electrocatalysts based on 3d transition metals (Co, Ni, Fe, *etc.*) for the OER due to their elemental abundance in the Earth's crust and similar valence electron structures of $3d^{6-8}4s^2$.[16] Among them, metal–organic frameworks (MOFs) have emerged as promising OER catalysts owing to their intrinsically large surface area and porosity.[15,17,18] In electrocatalysis, MOFs are usually utilized as precursors or sacrificial templates for the preparation of different electrocatalysts, such as metal sulfides,[19] nitrides[20] and carbides[21] by pyrolysis under various conditions. However, the attractive structural and compositional characteristics of precursors will be completely destroyed during pyrolysis, causing restricted active sites and blocked reactant transport.[22] Still, it is reasonable for MOFs to be used directly as (pre-)electrocatalysts to make the best of their distinctive properties. Nevertheless, the catalytic activity of pristine MOF materials is unsatisfactory, primarily on account of their poor inherent charge/mass transport capability.[23–25]

[a]*College of Chemistry, Chemical Engineering and Materials Science, Soochow University, Suzhou 215123, PR China. E-mail: duyk@suda.edu.cn*
[b]*Jiangsu Key Laboratory for Environment Functional Materials, School of Chemical Biology and Materials Engineering, Suzhou University of Science and Technology, Suzhou 215009, PR China. E-mail: zywu@mail.usts.edu.cn*

† Electronic supplementary information (ESI) available. See DOI: https://doi.org/10.1039/d2qi00125j

The inherently poor conductivity of MOFs limits their electrocatalytic applications. To address this issue, abundant studies have been devoted to enhancing the electrical conductivity of MOFs. The incorporation of metal chalcogenide and oxide nanoparticles into MOFs through a post-synthesis process and the creation of polymetallic MOFs with more open metal sites and an enriched electron environment could effectively enhance the electrical conductivity and electrocatalytic properties of MOFs.[26–30] Furthermore, MOFs with high electrical conductivity have also been developed by using ligands with a π-conjugated aromatic structure.[31,32] Mass transfer in MOFs is restricted by the mismatched porous size of MOFs for the diffusion of reactants. The large mass resistance results in low exposure and underutilization of the active sites. In this aspect, two-dimensional ultrathin nanosheet-like MOF materials are highly satisfactory and can be successfully developed by liquid–liquid interfacial growth, ultrasound-assisted exfoliation, sacrificial template growth, epitaxial growth, and other methods, which exhibit excellent electrocatalytic properties.[25,33,34]

Another superior strategy to improve the electrocatalytic activity of MOFs is the introduction of heterogeneous species into pristine MOFs.[35] In previous reports, tiny Ni_3S_2 or $CoFeO_x$ nanoparticles embedded in MOFs by post-synthetic plasma treatment were able to enhance the electrical conductivity and electrocatalytic performance of MOFs.[27,28] Such heterogeneous species can enhance the surface area and availability of active sites through modulating the nanostructure of MOFs. Moreover, they can also trigger probable synergistic effects between diverse constituents through the generation of interfacial electronic coupling, providing a huge opportunity to optimize the adsorption energy of key intermediates, thereby enhancing the inherent catalytic activity.[36–38]

Inspired by the above work, we report the CoFe-MS/MOF electrocatalyst formed by embedding metal sulfide particles into ultrathin Fe/Co-based MOF nanosheets using a facile one-step solvothermal method. It exhibits more outstanding OER electrocatalytic activity (10 mA cm^{-2} at 261 mV for the OER) than CoNi-MS/MOF, CoCu-MS/MOF, CoFe-MOF and (Fe)-Co_3S_4. It is found that the existence of iron/cobalt sulfide particles is essential to improving the electrocatalytic properties. Embedding sulfide particles in MOFs not only contributes to the formation of ultrathin nanosheets, but also effectively improves the electrical conductivity of the nanosheets and, more significantly, modulates the surface properties and electronic structure of the electrocatalysts, which together enhance the electrocatalytic activity.

2. Results and discussion

As illustrated in Fig. 1, the CoFe-MS/MOF nanosheets were synthesized in the presence of thioacetamide (TAA, a S source) and terephthalic acid (TPA, the MOF ligand) under solvothermal conditions with an input Fe^{3+}/Co^{2+} molar ratio of 1 : 4. For comparison, we also synthesized CoNi-MS/MOF and CoCu-MS/MOF nanosheets by the same method. The X-ray diffraction (XRD) pattern of the as-synthesized CoFe-MS/MOF (Fig. 2a) displays some characteristic diffraction peaks similar to those of the MOF-71 structure (no. 265 092, Cambridge Crystallographic Data Centre).[22,39] Two sharp diffraction peaks at 19.75° and 22.19° correspond to singlet sulfur (S, PDF#42-1278), probably due to the oxidation of sulfide in air. Some diffraction peaks at 16.37°, 32.14°, 38.33°, 47.21°, 50.53°, and 55.51° correspond to cobalt disulphide (Co_3S_4, PDF#47-1738), respectively.[26] The other diffraction peaks correspond to Fe_3S_4 (PDF#16-0713). This XRD pattern reveals that bimetallic sulfides and MOF-71 type MOFs coexist in the as-prepared CoFe-MS/MOF. As presented in the scanning electron microscopy (SEM) images of Fig. 2b and c, the CoFe-MS/MOF consists of a large number of ultrathin shuttle-shaped nanosheets (≈15–25 nm in thickness), and these ultrathin nanosheets

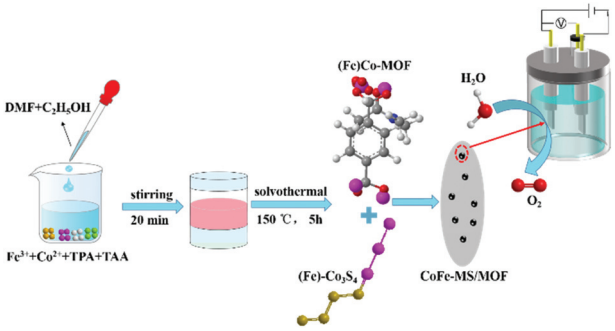

Fig. 1 Schematic diagram of the synthesis procedure for the CoFe-MS/MOF.

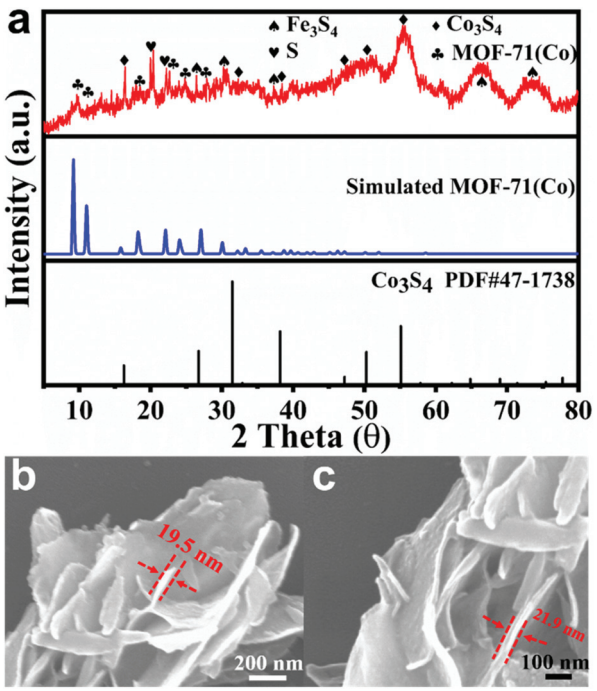

Fig. 2 (a) XRD patterns and (b and c) SEM images of the CoFe-MS/MOF.

form a large number of empty spaces by interconnecting and intersecting with each other. This distinctive open and layered porous structure facilitates mass transfer and provides highly specific surface areas for accelerating electrochemical reactions.[40–42]

To further investigate the microstructural characteristics of the CoFe-MS/MOF, transmission electron microscopy (TEM) tests were performed. The CoFe-MS/MOF is composed of various ultrathin nanosheets, as shown in the TEM image in Fig. 3a, which is consistent with the results observed by SEM. Compared to the CoNi-MS/MOF and CoCu-MS/MOF (Fig. S1†), the CoFe-MS/MOF with similar morphologies is significantly thinner. There were some black nanoparticles embedded in the ultrathin nanosheets (Fig. 3b), but no visible cracks, which implies good mechanical and electrical touch between various assemblies. The corresponding high-resolution TEM (HRTEM) image of the CoFe-MS/MOF (Fig. 3c) demonstrates the lattice *d*-spacing of approximately 0.209 and 0.254 nm, corresponding to the (400) and (422) lattices of Co_3S_4, agreeing well with the XRD pattern in Fig. 2a. It is noteworthy that no lattice stripes were observed for MOF-71, probably due to the disruption of the crystal structure of the MOF under a high-energy electron flow.[28,43]

The high-angle annular dark-field scanning TEM (HAADF-STEM) image (Fig. 3d) and corresponding energy-dispersive X-ray (EDX) mapping images (Fig. 3e) of a single CoFe-MS/MOF nanosheet display the even distribution of Co, Fe, O, and C elements and the discrete distribution of the S element throughout the entire nanosheet, indicating that metal sulfide particles are successfully embedded in the Fe/Co-based MOF nanosheet. The EDX spectrum (Fig. 3f) unveils an Fe/Co atomic ratio of approximately 1 : 6.9 in the nanosheet, which is marginally different from the Fe/Co ratio employed for the solvothermal reaction, probably due to the different coordination capabilities of Co^{2+} and Fe^{3+} during the MOF growth.[44] The EDX data of CoNi-MS/MOF and CoCu-MS/MOF are displayed in Fig. S2.†

To investigate the formation mechanism of this metal sulfide particle inlaid in MOF ultrathin nanosheets, a series of controlled experiments was conducted. In the absence of TAA or TPA, the products are referred to as CoFe-MOF and (Fe)-Co_3S_4, respectively. The control experiments revealed that the CoFe-MOF displays several characteristic peaks of the MOF-71 MOF without the peaks of metal sulfide, while pure metal sulfide (Fe)-Co_3S_4 is the opposite (Fig. S3†). In this situation, TAA releases S^{2-} ions as a vulcanization reagent to form bimetallic sulfides with the coexistence of Co_3S_4 and Fe_3S_4 under solvothermal conditions.[45] Additionally, the diffraction peak intensity of the metal sulfide is positively correlated with the TAA dosage at the same TPA dosage, indicating that the sulfide amount in the nanosheets can be tuned by the TAA content. Notably, both the shuttle-shaped CoFe-MOF and the hollow microspherical (Fe)-Co_3S_4 are thicker than the CoFe-MS/MOF (Fig. S4†), indicating that the inlaid sulfide in the Fe/Co-based MOF is conducive to the formation of ultrathin nanosheets. In the current situation, the diffraction peaks of the MOF are proved to be rather weak, whereas those of sulfide are proved to be intense for a shorter growth time. Consequently, we assume S^{2-} liberated by TAA first reacts with the metal (Co and Fe) ions to form sulfide nanomicrospheres, and is subsequently converted into metal sulfide particles inlaid in the MOF ultrathin nanosheets in the presence of TPA ligands.[46]

Among a series of bimetallic and monometallic catalysts, the optimized CoFe-MS/MOF catalyst synthesized with a 1 : 4 Fe/Co ratio after five hours of the solvothermal reaction displayed optimal OER activity in 1 M KOH (Fig. S5b and S6–S8†). As shown by the polarization curves in Fig. 4a, the CoFe-MS/MOF exhibits attractive OER activity as well as the lowest onset potential, which is significantly superior to those of the CoFe-MOF, (Fe)-Co_3S_4, CoCu-MS/MOF, CoNi-MS/MOF, and RuO_2. As shown in Fig. 4b, the CoFe-MS/MOF only demands a low overpotential of 261 mV to deliver a current density of 10 mA cm^{-2}, which is far smaller than those of the CoFe-MOF (312 mV), (Fe)-Co_3S_4 (306 mV), the CoNi-MS/MOF (305 mV), the CoCu-MS/MOF (299 mV), and commercial RuO_2 (313 mV).

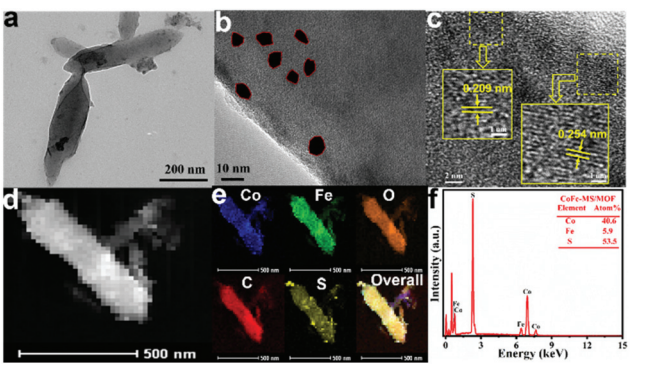

Fig. 3 (a) TEM image, (b and c) HRTEM images, (d) HAADF-STEM image, (e) the corresponding elemental mapping images of Co, Fe, O, C, and S, and (f) the SEM-EDX spectrum of the CoFe-MS/MOF nanosheet.

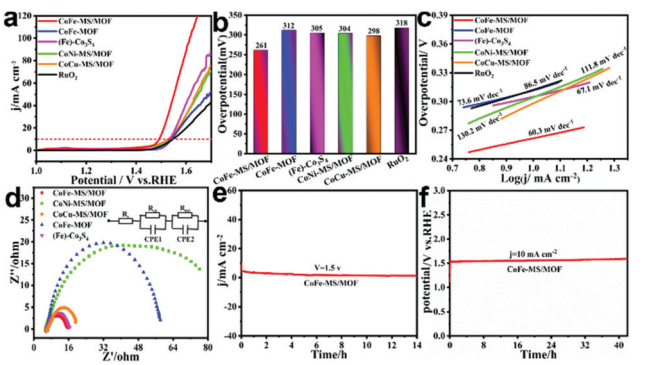

Fig. 4 Electrocatalytic OER activities in 1 M KOH. (a) Polarization curves, (b) histogram of overpotentials, and (c) Tafel plots at a current density of 10 mA cm^{-2}. (d) Nyquist plots. (e) The *i*–*t* curve under an overpotential of 270 mV over 14 h and (f) the prolonged chronopotentiometric curve over 40 h for the CoFe-MS/MOF.

Meanwhile, the CoFe-MS/MOF electrode also displays a smaller Tafel slope (60.3 mV dec^{-1}) than those of the CoFe-MOF (73.6 mV dec^{-1}), (Fe)-Co_3S_4 (67.1 mV dec^{-1}), the CoNi-MS/MOF (111.8 mV dec^{-1}), the CoCu-MS/MOF (130.2 mV dec^{-1}), and RuO_2 (86.5 mV dec^{-1}), which is shown in Fig. 4c, implying more beneficial OER kinetics. In addition, electrochemical impedance spectra (EIS) were measured to study the charge transport and conductivity of catalysts. As indicated in Fig. 4d, the Nyquist plots can be fitted using an equivalent circuit, and the corresponding fitted results are presented in Table S1.† The terms R_s, CPE, and R_{ct} represent the solution resistance, constant phase elements, and charge-transfer resistance, respectively. Obviously, the charge transfer resistance (R_{ct}) of the CoFe-MS/MOF is only 9.50 Ω, much smaller than those of the CoFe-MOF (51.80 Ω), (Fe)-Co_3S_4 (10.10 Ω), the CoNi-MS/MOF (72.92 Ω), and the CoCu-MS/MOF (14.60 Ω), suggesting faster OER kinetics of the CoFe-MS/MOF in comparison with that of the other four electrocatalysts. It primarily arises from the synergistic effect between the incorporated sulfide particles and the MOF, which diminishes the charge transfer resistance, and the ultrathin nanosheet structure, which shortens the electron transfer distance.[25,47] The above comparisons clearly disclose that embedding sulfide particles into MOF nanosheets can essentially improve the OER activity of the as-prepared CoFe-MS/MOF electrocatalyst. The CoFe-MS/MOF also exhibits excellent OER durability. As shown in the current density over time (i–t) curve in Fig. 4e, the current density exhibits a slow decline. Simultaneously, the chronoamperometric curve at a current density of 10 mA cm^{-2} reveals that the CoFe-MS/MOF remains quite durable after at least 40 h of continuous electrolysis (Fig. 4f), demonstrating superior durability toward the OER.

To investigate the possible origin of the considerably boosted water oxidation activity mentioned above, electrochemical surface areas (ECSAs) of the CoFe-MS/MOF, the CoFe-MOF, (Fe)-Co_3S_4, the CoNi-MS/MOF, and the CoCu-MS/MOF were compared through their double-layer capacitance (C_{dl}) (Fig. 5a and Fig. S8†).[48] As shown in Fig. 5b, the C_{dl} value of the CoFe-MS/MOF (7.71 mF cm^{-2}) is 2.6-, 4.7-, 4.0-, and 6.3-fold that of the CoFe-MOF, (Fe)-Co_3S_4, the CoNi-MS/MOF, and the CoCu-MS/MOF, individually, indicating a larger ECSA of the CoFe-MS/MOF, in accordance with the SEM and TEM observations. The electrocatalytic OER performance of the CoFe-MS/MOF and other comparison samples is listed in Table S2.† Nevertheless, the OER activity of the CoFe-MS/MOF fails to increase by a corresponding multiple, suggesting that it is not only determined by the increased ECSAs, but is also closely associated with the synergistic effect between the MOF nanosheets and the incorporated sulfide particles.

In order to illuminate the probable mechanism underlying such a synergistic effect, the alterations of the CoFe-MS/MOF in the structure and composition after electroactivation were investigated. After electrochemical activation (usually 20 cycles between 1.0 and 1.7 V (*vs.* RHE) at 10 mV s^{-1}), the diffraction peaks of the metal sulfide show no remarkable difference, while those of the MOF entirely vanish, as displayed by the XRD pattern in Fig. 6a. This indicates that the crystal structure of the MOF nanosheets has undergone a transformation during the electroactivation process, whereas the sulfide particles survive, as evidenced by the Raman spectra (Fig. 6b).[30,49] The survival of the sulfide particles is possibly due to the fact that they are sheltered from the phase changes during electroactivation by the surrounding oxyhydroxide substrate. The nanosheet morphology of the CoFe-MS/MOF remains invariant, yet its thickness is significantly enlarged (Fig. 6c and d), indicating the formation of (oxy)hydroxides during electrochemical activation, which act as the actual active sites of the OER.[26,50,51]

X-ray photoelectron spectroscopy (XPS) was performed to examine the electronic interactions in the CoFe-MS/MOF. The survey spectrum of the CoFe-MS/MOF reveals the existence of Co, Fe, S, O, and C elements, as shown in Fig. 7a. The O 1s spectrum of the CoFe-MS/MOF in Fig. 7b displays three subpeaks assigned to a M–O bond, a carboxyl (O═C–O–) bond, as well as the absorbed water. After electrochemical activation, the proportion of carboxyl O apparently decreases, whereas the M–O bonds grow, indicating the transformation of the MOF to

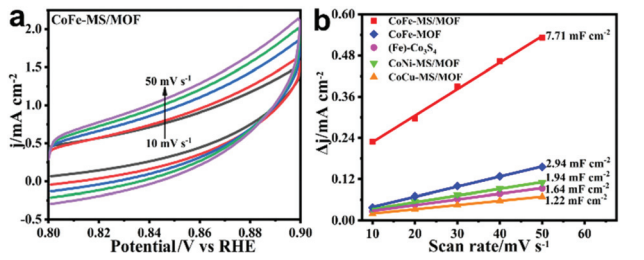

Fig. 5 (a) Cyclic voltammograms of the CoFe-MS/MOF. (b) Double layer currents of different catalysts *versus* the scan rate.

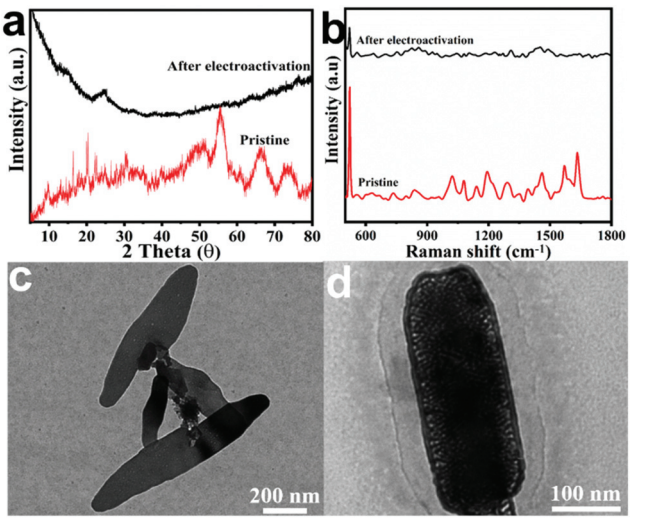

Fig. 6 (a) XRD patterns and (b) Raman spectra of the CoFe-MS/MOF before and after electrochemical activation. (c and d) TEM images of the CoFe-MS/MOF after electrochemical activation.

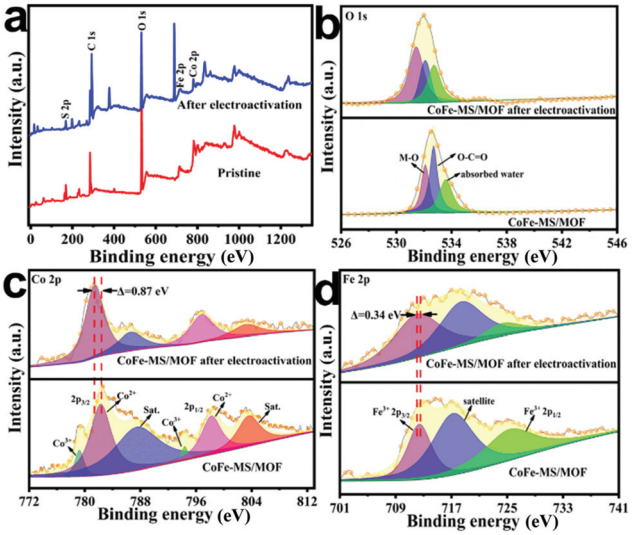

Fig. 7 (a) XPS survey spectra and (b) O 1s, (c) Co 2p, and (d) Fe 2p spectra of the CoFe-MS/MOF before and after electrochemical activation.

oxyhydroxide during the OER process. Fig. 7c shows the Co 2p spectra from the CoFe-MS/MOF before and after electroactivation. The binding energies of 781.80 (Co $2p_{3/2}$) and 797.70 eV (Co $2p_{1/2}$) correspond to the Co^{2+} species, and 778.73 (Co $2p_{3/2}$) and 793.87 eV (Co $2p_{1/2}$) are associated with surface-oxidized Co^{3+}, respectively.[52] It is notable that the binding energy of Co $2p_{3/2}$ for the CoFe-MS/MOF decreases after electrochemical activation (ΔBE = 0.87 eV). The peaks at 711.90 ($2p_{3/2}$) and 724.83 eV ($2p_{1/2}$) are indexed to Fe^{3+} and a resembling binding energy shift is noted in the Fe 2p spectra as well (Fig. 7d).[49] This indicates that their electronic structure is apparently altered to an electron-rich state by the metal sites in the CoFe-MS/MOF after electrochemical activation. It is caused by metal sulfide particles conferring electrons from their electron-rich metal atoms to the surface Co and Fe centers.[51,53,54]

Recent studies further indicate that the OER activity of Fe/Co-based catalysts can be boosted through enhancing the adsorption of oxygenated intermediates such as *OH and *O on the surface.[35,55,56] As shown in Fig. 4c and d, the Fe/Co centers at the electron-rich state favor the enhancement of oxygen-containing intermediates for expedited OER kinetics,[16,57] evidenced by the smaller R_{ct} and smaller Tafel slope of the CoFe-MS/MOF in comparison with the CoFe-MOF in this work. Thus, a greater inherent OER activity of the CoFe-MS/MOF stems from the larger electron density at its metal sites, which is caused by the embedded metal sulfide particles.

To estimate the application of the CoFe-MS/MOF as a remarkable OER catalyst in a water-splitting cell, the overall electrocatalytic water decomposition performance of the CoFe-MS/MOF was investigated herein. The CoFe-MS/MOF and the commercial Pt/C catalyst serve as the anodic and cathodic working electrodes (WE) of a double-electrode cell in 1 M KOH, respectively (Fig. 8a). From the polarization curve

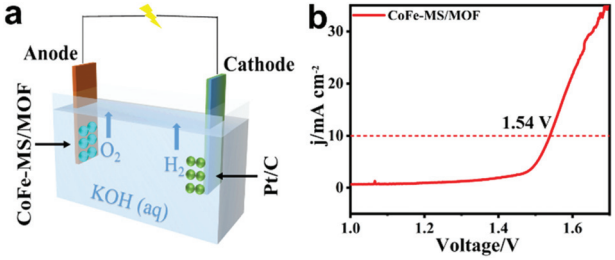

Fig. 8 (a) The schematic diagram of the overall water splitting based on CoFe-MS/MOF//Pt/C electrodes. (b) Polarization curve of the overall water splitting over the CoFe-MS/MOF//Pt/C two-electrode couple.

(Fig. 8b), it is unambiguously discovered that this CoFe-MS/MOF//Pt/C couple entails a smaller cell voltage of 1.54 V in comparison with the RuO_2//Pt/C couple to achieve a current density of 10 mA cm^{-2}, reflecting its promising application toward water splitting.

3. Conclusions

To sum up, a range of CoM (M = Fe, Ni, Cu)-MS/MOF, CoFe-MOF, and (Fe)-Co_3S_4 samples was successfully synthesized through a facile one-step solvothermal method. Among these, the as-prepared CoFe-MS/MOF consisting of interconnected MOF ultrathin nanosheets with metal sulfide nanoparticles exhibits a much lower overpotential, smaller Tafel slope, and excellent stability, which indicate its greatly improved OER activity in alkaline conditions. Furthermore, by coupling with Pt/C, the CoFe-MS/MOF is able to drive water splitting to deliver a current density of 10 mA cm^{-2} with an ultralow cell voltage of 1.54 V as well, indicating the promising application of the CoFe-MS/MOF for overall water splitting. The boosting mechanism results from the metal sulfide particles embedded in the nanosheets, which facilitates the formation of ultrathin nanosheets to significantly expand the ECSAs, while providing high electrical conductivity but, more significantly, effectively regulates the electronic structure of the catalytically active atomic sites to an electron-rich state through strong electronic interactions, enhancing the adsorption of O-containing intermediates to promote rapid electrochemical reactions. This research offers prospects for the sensible design of high-performance and cost-effective bimetallic sulfide doped MOF materials for electrocatalytic applications.

Conflicts of interest

There are no conflicts to declare.

Acknowledgements

The authors thank the National Natural Science Foundation of China (Grant No. 52073199 and 51873136).

Notes and references

1 H. Xu, Y. Zhao, Q. Wang, G. He and H. Chen, Supports promote single-atom catalysts toward advanced electrocatalysis, *Coord. Chem. Rev.*, 2022, **451**, 214261–214268.

2 J. Li, C. Wang, H. Shang, Y. Wang, H. You, H. Xu and Y. Du, Metal-modified $PtTe_2$ nanorods: surface reconstruction for efficient methanol oxidation electrocatalysis, *Chem. Eng. J.*, 2021, **424**, 130319.

3 H. Xu, Y. Zhao, G. He and H. Chen, Race on engineering noble metal single-atom electrocatalysts for water splitting, *Int. J. Hydrogen Energy*, 2022, **47**, 14257–14279.

4 R. Yu, D. Liu, M. Yuan, Y. Wang, C. Ye, J. Li and Y. Du, Universal MOF-Mediated synthesis of 2D CoNi-based layered triple hydroxides electrocatalyst for efficient oxygen evolution reaction, *J. Colloid Interface Sci.*, 2021, **602**, 612–618.

5 P. Zhai, M. Xia, Y. Wu, G. Zhang, J. Gao, B. Zhang, S. Cao, Y. Zhang, Z. Li, Z. Fan, C. Wang, X. Zhang, J. T. Miller, L. Sun and J. Hou, Engineering single-atomic ruthenium catalytic sites on defective nickel-iron layered double hydroxide for overall water splitting, *Nat. Commun.*, 2021, **12**, 1–11.

6 Q. Mou, Z. Xu, G. Wang, E. Li, J. Liu, P. Zhao, X. Liu, H. Li and G. Cheng, A bimetal hierarchical layer structure MOF grown on Ni foam as a bifunctional catalyst for the OER and HER, *Inorg. Chem. Front.*, 2021, **8**, 2889–2899.

7 H. Xu, H. Shang, C. Wang and Y. Du, Low–dimensional metallic nanomaterials for advanced electrocatalysis, *Adv. Funct. Mater.*, 2020, **30**, 2006317.

8 Z. Li, X. Xu, X. Lu, C. He, J. Huang, W. Sun and L. Tian, Synergistic coupling of $FeNi_3$ alloy with graphene carbon dots for advanced oxygen evolution reaction electrocatalysis, *J. Colloid Interface Sci.*, 2022, **615**, 273–281.

9 J. Wang, S.-J. Kim, J. Liu, Y. Gao, S. Choi, J. Han, H. Shin, S. Jo, J. Kim, F. Ciucci, H. Kim, Q. Li, W. Yang, X. Long, S. Yang, S.-P. Cho, K. H. Chae, M. G. Kim, H. Kim and J. Lim, Redirecting dynamic surface restructuring of a layered transition metal oxide catalyst for superior water oxidation, *Nat. Catal.*, 2021, **4**, 212–222.

10 Y. Wang, C. Wang, H. Shang, M. Yuan, Z. Wu, J. Li and Y. Du, Self-driven Ru-modified NiFe MOF nanosheet as multifunctional electrocatalyst for boosting water and urea electrolysis, *J. Colloid Interface Sci.*, 2022, **605**, 779–789.

11 C. Wang, H. Shang, Y. Wang, H. Xu, J. Li and Y. Du, Interfacial electronic structure modulation enables $CoMoO_x/CoO_x/RuO_x$ to boost advanced oxygen evolution electrocatalysis, *J. Mater. Chem. A*, 2021, **9**, 14601–14606.

12 R. K. Hona, S. B. Karki, T. Cao, R. Mishra, G. E. Sterbinsky and F. Ramezanipour, Sustainable oxide electrocatalyst for hydrogen- and oxygen-evolution reactions, *ACS Catal.*, 2021, **11**, 14605–14614.

13 C. Cai, S. Han, Q. Wang and M. Gu, Direct observation of yolk-shell transforming to gold single atoms and clusters with superior oxygen evolution reaction efficiency, *ACS Nano*, 2019, **13**, 8865–8871.

14 J. Qi, Y. P. Lin, D. Chen, T. Zhou, W. Zhang and R. Cao, Autologous cobalt phosphates with modulated coordination sites for electrocatalytic water oxidation, *Angew. Chem., Int. Ed.*, 2020, **59**, 8917–8921.

15 S. Pan, X. Mao, J. Yu, L. Hao, A. Du and B. Li, Remarkably improved oxygen evolution reaction activity of cobalt oxides by an Fe ion solution immersion process, *Inorg. Chem. Front.*, 2020, **7**, 3327–3339.

16 T. Wu, X. Ren, Y. Sun, S. Sun, G. Xian, G. G. Scherer, A. C. Fisher, D. Mandler, J. W. Ager, A. Grimaud, J. Wang, C. Shen, H. Yang, J. Gracia, H. J. Gao and Z. J. Xu, Spin pinning effect to reconstructed oxyhydroxide layer on ferromagnetic oxides for enhanced water oxidation, *Nat. Commun.*, 2021, **12**, 3634.

17 X. Wang, X. Wang, L. Zhao, H. Zhang, M. Liu, C. Zhang and S. Liu, Self-reconstruction of cationic activated Ni-MOFs enhanced the intrinsic activity of electrocatalytic water oxidation, *Inorg. Chem. Front.*, 2022, **9**, 179–185.

18 C. Wang, H. Shang, J. Li, Y. Wang, H. Xu, C. Wang, J. Guo and Y. Du, Ultralow Ru doping induced interface engineering in MOF derived ruthenium-cobalt oxide hollow nanobox for efficient water oxidation electrocatalysis, *Chem. Eng. J.*, 2021, **420**, 129805.

19 K. Berijani and A. Morsali, The role of metal–organic porous frameworks in dual catalysis, *Inorg. Chem. Front.*, 2021, **8**, 3618–3658.

20 Y. Gu, S. Chen, J. Ren, Y. A. Jia, C. Chen, S. Komarneni, D. Yang and X. Yao, Electronic structure tuning in Ni_3FeN/r-GO aerogel toward bifunctional electrocatalyst for overall water splitting, *ACS Nano*, 2018, **12**, 245–253.

21 Y. Lv and J. R. Gong, In situ growth of MOF-derived ultrafine molybdenum carbide nanoparticles supported on Ni foam as efficient hydrogen-evolution electrocatalysts, *J. Mater. Chem. A*, 2021, **9**, 15246–15253.

22 M. Zhao, T. Guo, W. Qian, Z. Wang, X. Zhao, L. Wen and D. He, Fe-incorporated cobalt-based metal-organic framework ultrathin nanosheets for electrocatalytic oxygen evolution, *Chem. Eng. J.*, 2021, **422**, 130055.

23 Q. Liang, J. Chen, F. Wang and Y. Li, Transition metal-based metal-organic frameworks for oxygen evolution reaction, *Coord. Chem. Rev.*, 2020, **424**, 213488.

24 C. Meng, Y. Cao, Y. Luo, F. Zhang, Q. Kong, A. A. Alshehri, K. A. Alzahrani, T. Li, Q. Liu and X. Sun, A Ni-MOF nanosheet array for efficient oxygen evolution electrocatalysis in alkaline media, *Inorg. Chem. Front.*, 2021, **8**, 3007–3011.

25 Z. Li, C. Li, J. Huang, W. Sun, W. Cheng, C. He and L. Tian, Structure engineering of amorphous P–CoS hollow electrocatalysts for promoted oxygen evolution reaction, *Int. J. Hydrogen Energy*, 2022, **47**, 15189–15197.

26 M. Wang, C.-L. Dong, Y.-C. Huang and S. Shen, Operando spectral and electrochemical investigation into the heterophase stimulated active species transformation in transition-metal sulfides for efficient electrocatalytic oxygen evolution, *ACS Catal.*, 2020, **10**, 1855–1864.

27 W. Zhang, Y. Wang, H. Zheng, R. Li, Y. Tang, B. Li, C. Zhu, L. You, M. R. Gao, Z. Liu, S. H. Yu and K. Zhou,

Embedding ultrafine metal oxide nanoparticles in monolayered metal-organic framework nanosheets enables efficient electrocatalytic oxygen evolution, *ACS Nano*, 2020, **14**, 1971–1981.

28 M. Zhao, W. Li, J. Li, W. Hu and C. M. Li, Strong electronic interaction enhanced electrocatalysis of metal sulfide clusters embedded metal-organic framework ultrathin nanosheets toward highly efficient overall water splitting, *Adv. Sci.*, 2020, **7**, 2001965.

29 H. Su, S. Song, S. Li, Y. Gao, L. Ge, W. Song, T. Ma and J. Liu, High-valent bimetal Ni_3S_2/Co_3S_4 induced by Cu doping for bifunctional electrocatalytic water splitting, *Appl. Catal., B*, 2021, **293**, 120225.

30 M. Xie, Y. Ma, D. Lin, C. Xu, F. Xie and W. Zeng, Bimetal-organic framework MIL-53(Co-Fe): an efficient and robust electrocatalyst for the oxygen evolution reaction, *Nanoscale*, 2020, **12**, 67–71.

31 H. Zhong, K. H. Ly, M. Wang, Y. Krupskaya, X. Han, J. Zhang, J. Zhang, V. Kataev, B. Buchner, I. M. Weidinger, S. Kaskel, P. Liu, M. Chen, R. Dong and X. Feng, A phthalocyanine-based layered two-dimensional conjugated metal-organic framework as a highly efficient electrocatalyst for the oxygen reduction reaction, *Angew. Chem., Int. Ed.*, 2019, **58**, 10677–10682.

32 S. S. Shinde, C. H. Lee, J.-Y. Jung, N. K. Wagh, S.-H. Kim, D.-H. Kim, C. Lin, S. U. Lee and J.-H. Lee, Unveiling dual-linkage 3D hexaiminobenzene metal–organic frameworks towards long-lasting advanced reversible Zn–air batteries, *Energy Environ. Sci.*, 2019, **12**, 727–738.

33 Y. Lin, H. Wan, D. Wu, G. Chen, N. Zhang, X. Liu, J. Li, Y. Cao, G. Qiu and R. Ma, Metal-organic framework hexagonal nanoplates: bottom-up synthesis, topotactic transformation, and efficient oxygen evolution reaction, *J. Am. Chem. Soc.*, 2020, **142**, 7317–7321.

34 Z. Li, D. Liu, X. Lu, M. Du, Z. Chen, J. Teng, R. Sha and L. Tian, Boosting oxygen evolution of layered double hydroxide through electronic coupling with ultralow noble metal doping, *Dalton Trans.*, 2022, **51**, 1527–1532.

35 N. Han, S. Luo, C. Deng, S. Zhu, Q. Xu and Y. Min, Defect-rich $FeN_{0.023}/Mo_2C$ heterostructure as a highly efficient bifunctional catalyst for overall water-splitting, *ACS Appl. Mater. Interfaces*, 2021, **13**, 8306–8314.

36 Q. Zhang, M. Zhang, T. Chen, L. Li, S. Shi and R. Jiang, Unconventional phase engineering of fuel-cell electrocatalysts, *J. Electroanal. Chem.*, 2022, **916**, 116363.

37 Y. Huang, G. Wei, J. He, C. An, M. Hu, M. Shu, J. Zhu, S. Yao, W. Xi, R. Si, Z.-M. Zhang and C. An, Interfacial electronic interaction of atomically dispersed IrClx on ultrathin $Co(OH)_2$/CNTs for efficient electrocatalytic water oxidation, *Appl. Catal., B*, 2020, **279**, 119398.

38 H. Xu, B. Huang, Y. Zhao, G. He and H. Chen, Engineering Heterostructured Pd–Bi_2Te_3 Doughnut/Pd Hollow Nanospheres for Ethylene Glycol Electrooxidation, *Inorg. Chem.*, 2022, **61**, 4533–4540.

39 N. L. Rosi, J. Kim, M. Eddaoudi, B. Chen, M. O'Keeffe and O. M. Yaghi, Rod packings and metal–organic frameworks constructed from rod-shaped secondary building units, *J. Am. Chem. Soc.*, 2005, **127**, 1504–1518.

40 X. Zhu, J. Dai, L. Li, D. Zhao, Z. Wu, Z. Tang, L.-J. Ma and S. Chen, Hierarchical carbon microflowers supported defect-rich Co_3S_4 nanoparticles: An efficient electrocatalyst for water splitting, *Carbon*, 2020, **160**, 133–144.

41 Z. Ye, Y. Jiang, L. Li, F. Wu and R. Chen, A high-efficiency CoSe electrocatalyst with hierarchical porous polyhedron nanoarchitecture for accelerating polysulfides conversion in Li-S batteries, *Adv. Mater.*, 2020, **32**, 2002168.

42 L. Yang, L. Zeng, H. Liu, Y. Deng, Z. Zhou, J. Yu, H. Liu and W. Zhou, Hierarchical microsphere of MoNi porous nanosheets as electrocatalyst and cocatalyst for hydrogen evolution reaction, *Appl. Catal., B*, 2019, **249**, 98–105.

43 Z. Zou, T. Wang, X. Zhao, W.-J. Jiang, H. Pan, D. Gao and C. Xu, Expediting in-Situ electrochemical activation of two-dimensional metal–organic frameworks for enhanced OER intrinsic activity by iron incorporation, *ACS Catal.*, 2019, **9**, 7356–7364.

44 J. Xu, X. Zhu and X. Jia, From low- to high-crystallinity bimetal–organic framework nanosheet with highly exposed boundaries: an efficient and stable electrocatalyst for oxygen evolution reaction, *ACS Sustainable Chem. Eng.*, 2019, **7**, 16629–16639.

45 Y. Guo, J. Tang, H. Qian, Z. Wang and Y. Yamauchi, One-pot synthesis of zeolitic imidazolate framework 67-derived hollow Co_3S_4@MoS_2 heterostructures as efficient bifunctional catalysts, *Chem. Mater.*, 2017, **29**, 5566–5573.

46 X. Zhang, B. Li, M. Lan, S. Yang, Q. Xie, J. Xiao, F. Xiao and S. Wang, Cation modulation of cobalt sulfide supported by mesopore-rich hydrangea-like carbon nanoflower for oxygen electrocatalysis, *ACS Appl. Mater. Interfaces*, 2021, **13**, 18683–18692.

47 G. Zhang, Y. Li, X. Xiao, Y. Shan, Y. Bai, H. G. Xue, H. Pang, Z. Tian and Q. Xu, In situ anchoring polymetallic phosphide nanoparticles within porous prussian blue analogue nanocages for boosting oxygen evolution catalysis, *Nano Lett.*, 2021, **21**, 3016–3025.

48 S. Niu, W. J. Jiang, Z. Wei, T. Tang, J. Ma, J. S. Hu and L. J. Wan, Se-doping activates FeOOH for cost-effective and efficient electrochemical water oxidation, *J. Am. Chem. Soc.*, 2019, **141**, 7005–7013.

49 K. Ge, S. Sun, Y. Zhao, K. Yang, S. Wang, Z. Zhang, J. Cao, Y. Yang, Y. Zhang, M. Pan and L. Zhu, Facile synthesis of two-dimensional iron/cobalt metal-organic framework for efficient oxygen evolution electrocatalysis, *Angew. Chem., Int. Ed.*, 2021, **60**, 12097–12102.

50 X. Chen, D.-D. Ma, B. Chen, K. Zhang, R. Zou, X.-T. Wu and Q.-L. Zhu, Metal–organic framework-derived mesoporous carbon nanoframes embedded with atomically dispersed Fe–N active sites for efficient bifunctional oxygen and carbon dioxide electroreduction, *Appl. Catal., B*, 2020, **267**, 118720.

51 T. I. Singh, G. Rajeshkhanna, U. N. Pan, T. Kshetri, H. Lin, N. H. Kim and J. H. Lee, Alkaline water splitting enhancement by MOF-derived Fe-Co-oxide/Co@NC-mNS hetero-

structure: boosting OER and HER through defect engineering and in situ oxidation, *Small*, 2021, **17**, 2101312.
52 M. Arif, G. Yasin, L. Luo, W. Ye, M. A. Mushtaq, X. Fang, X. Xiang, S. Ji and D. Yan, Hierarchical hollow nanotubes of NiFeV-layered double hydroxides@CoVP heterostructures towards efficient, pH-universal electrocatalytical nitrogen reduction reaction to ammonia, *Appl. Catal., B*, 2020, **265**, 118559.
53 H. Xu, H. Shang, C. Wang and Y. Du, Surface and interface engineering of noble-metal-free electrocatalysts for efficient overall water splitting, *Coord. Chem. Rev.*, 2020, **418**, 213374.
54 C. Wang, L. Jin, H. Shang, H. Xu, Y. Shiraishi and Y. Du, Advances in engineering RuO_2 electrocatalysts towards oxygen evolution reaction, *Chin. Chem. Lett.*, 2021, **32**, 2108–2116.
55 G. Barati Darband, M. Aliofkhazraei, S. Hyun, A. Sabour Rouhaghdam and S. Shanmugam, Electrodeposition of Ni-Co-Fe mixed sulfide ultrathin nanosheets on Ni nanocones: a low-cost, durable and high performance catalyst for electrochemical water splitting, *Nanoscale*, 2019, **11**, 16621–16634.
56 C. Wang, H. Xu, Y. Wang, H. Shang, L. Jin, F. Ren, T. Song, J. Guo and Y. Du, Hollow V-doped CoMx (M = P, S, O) nanoboxes as efficient OER electrocatalysts for overall water splitting, *Inorg. Chem.*, 2020, **59**, 11814–11822.
57 W. J. Jiang, T. Tang, Y. Zhang and J. S. Hu, Synergistic modulation of non-precious-metal electrocatalysts for advanced water splitting, *Acc. Chem. Res.*, 2020, **53**, 1111–1123.